ACS OMEGA

http://pubs.acs.org/journal/acsodf

Article

Self-Assembly of Triple-Stranded Lanthanide Molecular Quasi-Lantern Containing 2,2′-Bipyridine Receptor: Luminescence Sensing and Magnetic Property

Fan Yin, Zhi Liu, Jian Yang, Li-Peng Zhou, Chong-Bin Tian,* and Qing-Fu Sun*

Cite This: *ACS Omega* 2023, 8, 24477−24484

Read Online

ACCESS | Metrics & More | Article Recommendations | Supporting Information

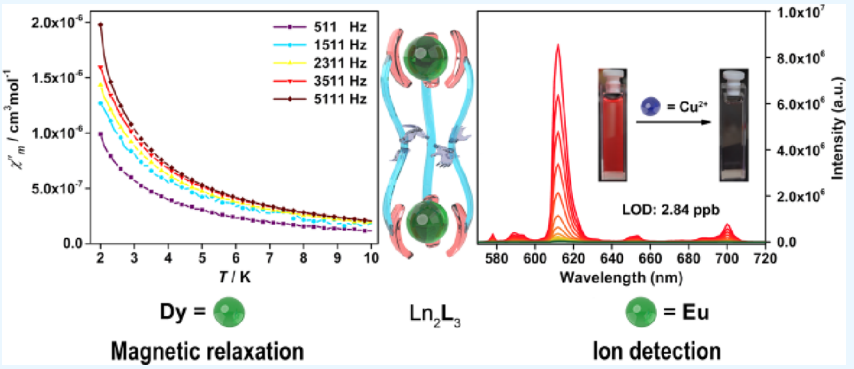

ABSTRACT: Ln_2L_3-type supramolecular architectures have received significant attention recently due to their unique magnetism and optical properties. Herein, we report the triple-stranded Ln_2L_3-type lanthanide molecular quasi-lanterns, which are fabricated by the deprotonation self-assembly of a linear ligand featuring a β-diketone chelating claw and 2,2′-bipyridine (bpy) moiety with lanthanide ions (Ln = Eu^{3+} and Dy^{3+}). The crystal structure analysis indicates that Eu^{3+} and Dy^{3+} ions are all coordinated by eight oxygen donors but in different coordination geometries. The eight oxygen donors in Eu_2L_3 and Dy_2L_3 are arranged in a square antiprism and triangular dodecahedron geometry, respectively. Taking into account the fact that the bpy moiety has a strong coordination affinity for transition metal ions, luminescence sensing toward Cu^{2+} ions has been demonstrated with Eu_2L_3, bearing a detection of limit as low as 2.84 ppb. The luminescence sensing behavior of Eu_2L_3 is ascribed to the formation host−guest complex between Eu_2L_3 and Cu^{2+} ions with a 1:2 binding ratio. Dynamic AC susceptibility measurements for Dy_2L_3 reveal the relaxation of magnetization in it. This work provides a potential way for design and fabrication of lanthanide-based molecular materials with functions endowed by the ligands.

INTRODUCTION

Over the past few decades, discrete architectures generated by the coordination-directed self-assembly approach, including macrocycles, planes, knots, and polyhedra, have experienced rapid and violent development and have been one of the most active research areas of supramolecular chemistry.[1−9] Among these architectures, the dinuclear M_2L_3-type (M, metal; L, ligand) triple-stranded helicates or lantern-like metalla-cages formed by the self-assembly of C_2-symmetric ligands with metal centers are particularly appealing due to their potential applications in the field of magnetism,[10−12] luminescence,[13−16] bionics,[17,18] catalysis,[19,20] encapsulation,[21,22] selective separation and recognition,[23] and so on. Since Lehn and co-workers introduced the term helicate into supramolecular chemistry in 1987,[24] a considerable number of M_2L_3-type architectures bearing triple-stranded helicate or lantern-like morphologies have been developed.[25−28] As far as we are aware, most of such M_2L_3-type architectures were fabricated by transition metals and only a few cases by lanthanides.[27,29] This is not surprising if we consider that lanthanides usually have high kinetic lability, weak coordination ability, variable coordination numbers, and lack of stereochemical affinity compared with the transition metals containing a strong coordination-directed feature. All those shortcomings make it difficult to construct Ln_2L_3-type (Ln, lanthanide) architectures. Despite this, the construction of Ln_2L_3-type assemblies deserves to be explored as the intrinsic properties of lanthanides, such as magnetism and optics, have shown to be excellent candidates as single molecular magnets and luminescence sensors.[30−34] In the

Received: April 10, 2023
Accepted: June 13, 2023
Published: June 29, 2023

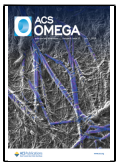

efforts of Piguet et al.,[25,35,36] Bünzli et al.,[37,38] Hamacek et al.,[39] Hooley et al.,[40,41] Duan et al.,[42,43] Yan et al.,[44,45] our group,[21,46,47] and others,[48−51] several Ln_2L_3-type assemblies had been reported. To date, such reports are mainly focused on the investigation of chiral, luminescence, structure evolution, and aggregation of Ln_2L_3, while other functional explorations are still in their initial stage, in particular for the function stemming from the ligands.

It had been realized that the 2,2′-bipyridine (bpy) moiety is an excellent metal chelator in coordination polymer or metal−organic framework synthesis and can be adopted as a sensor when it is on its own as a luminescence emitting center or in combination with other luminescence emitting centers.[52−56] Additionally, the β-diketone chelating claw can well sensitize the luminescence emission of Eu^{3+} ions[15] and once complexation with Dy^{3+} ions is likely to afford the single-molecular magnet (SMM) behavior.[31,57] By combining the bpy moiety and β-diketone chelating claw into one ligand, the recognition toward transition metals and possible SMM properties can be anticipated upon complexation with corresponding lanthanides. Bearing this in mind, herein, a new Ligand H_2L was designed by incorporating the bpy moiety into a C_2-symmetric linear shape ligand with two β-diketone chelating claws located at the two ends. After assembly of H_2L with Ln (Ln = Eu^{3+} and Dy^{3+}) ions, the triple-stranded Ln_2L_3 assemblies bearing an elongated lantern-like architecture were obtained. The luminescence probe for sensing Cu^{2+} ions has been demonstrated on Eu_2L_3 assembly, which is attributed to the coordination of Cu^{2+} ions with free bpy sites. Moreover, alternating current susceptibility measurements under a zero dc field indicate that Dy_2L_3 shows magnetic relaxation.

RESULTS AND DISCUSSION

Ligand Design and Synthesis. The ligand H_2L containing the 2,2′-bipyridine functional unit was prepared by a multi-step procedure, as shown in Scheme S1, and characterized by NMR. Compound 5,5′-bis(bromomethyl)-2,2′-bipyridine was synthesized according to the reported procedures.[58] The 5,5′-bis(bromomethyl)-2,2′-bipyridine was reacted with *p*-hydroxyacetophenone via nucleophilic substitution reaction, leading to the formation of intermediate 5,5′-bis-4-acetylphenoxymethyl-2,2′-bipyridine. The ligand H_2L was then obtained after Claisen condensation of this intermediate with methyl trifluoroacetate. The experimental details can be found in the Supporting Information (Figures S1−S5).

Self-Assembly and Characterization of Eu_2L_3. The Eu_2L_3 was synthetized by the assembly of ligand H_2L and $Eu(OTf)_3$ in a molar ratio of 3:2 with the trimethylamine (Et_3N) as the base in methanol (Scheme 1). The ^1H NMR spectrum suggests the formation of a single complex with a high degree of symmetry. Compared with the free ligand, all signals arising from the triple-stranded Eu_2L_3 (Figure 1B) assembly are minutely shifted downfield and broadening due to the coordination with weak paramagnetic Eu^{3+} ions, which can be attributed to lanthanide-induced shifts (LIS) and relaxation rate enhancement (LIR) effect.[13,59] The high symmetry of the Eu_2L_3 is further confirmed by $^1H-^1H$ COSY spectra (Figure S7), which indicates that three ligands on the Eu_2L_3 share identical magnetic-chemical environments in DMSO-d_6.

Besides the observed triple-stranded Eu_2L_3 architecture, another possible architecture constructed by such bidentate linear ligand H_2L is quadruply stranded Eu_2L_4. To gain the

Scheme 1. Synthetic Route of the Ln_2L_3[a]

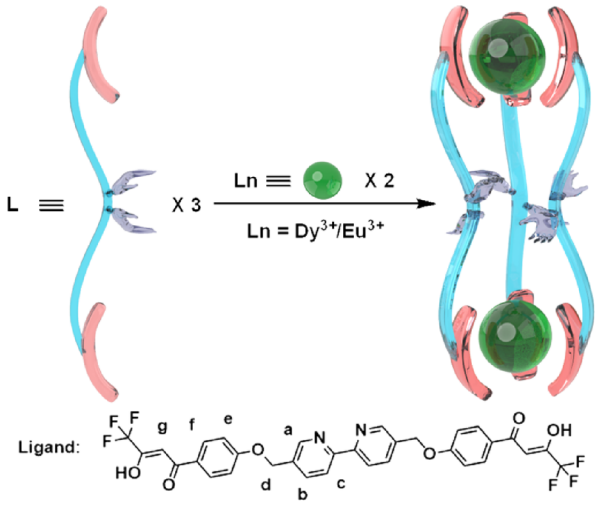

[a]Light red: coordination oxygen atoms, light blue hand: bpy, sky blue: the ligand backbones, green: lanthanide ions.

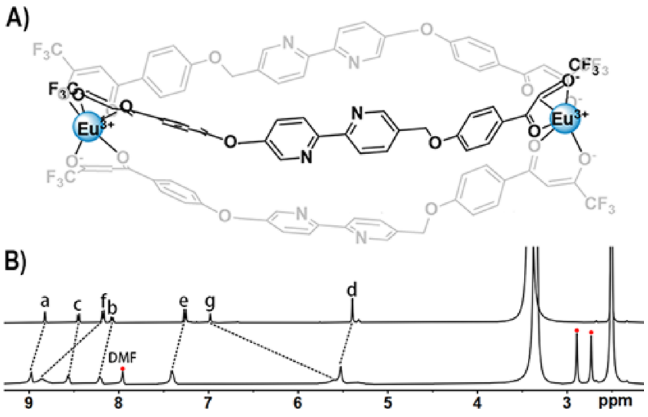

Figure 1. (A) Molecular structure diagram of Eu_2L_3. (B) ^1H NMR (400 MHz, 298 K) of H_2L and Eu_2L_3 in DMSO-d_6.

possible species Eu_2L_4, the ratio of H_2L to metal ions (Eu^{3+}) increased from 3:2 to 4:2. Unfortunately, the assembly of H_2L, $Eu(OTf)_3$, and Et_3N in 4:2:8 stoichiometry afforded Eu_2L_3 other than Eu_2L_4, as suggested by its ^1H-NMR spectrum, which is identical with the Eu_2L_3 (Figure S8). This result is significantly different with the observation of Yan et al.[14] that the quadruply stranded lanthanide structure can be formed by mixing the similar ligand with Ln^{3+} in 4:2 stoichiometry. The difference between H_2L and Yan et al.'s ligand lies in their linker. In comparison to the flexible 1,2-propanediol linker in Yan et al.'s ligand, the linker in H_2L was relative rigid bpy, which gives rise to the decreased flexibility of H_2L over Yan et al.'s ligand. Such decreased flexibility should be responsible for the formation of the Eu_2L_3 architecture instead of the four-stranded Eu_2L_4 architecture. Therefore, it can be inferred that the flexible feature of the ligand linker plays an important role in determining the formation of triple-stranded Ln_2L_3 or quadruply stranded Ln_2L_4.

Crystal Structure Description. Slow volatilization of the Eu_2L_3 DMF solution at room temperature for 3 months results in the generation of colorless plate-like single crystals Eu_2L_3, which were suitable for X-ray diffraction measurement. To shorten the crystal growth time, Dy_2L_3 single crystals were

https://doi.org/10.1021/acsomega.3c02419
ACS Omega 2023, 8, 24477−24484

prepared by slow vapor diffusion of CH_2Cl_2 into the DMSO solution of Dy_2L_3 for about 2 weeks. Single-crystal X-ray diffraction analysis indicates that both of Eu_2L_3 and Dy_2L_3 are isomorphous compounds, crystallizing in the space group *P*-1 with $Z = 2$ and featuring an elongated lantern-like triple-stranded core structure with different coordination solvents, i.e., DMF for Eu_2L_3 and DMSO for Dy_2L_3. Therefore, the structure description of compound Eu_2L_3 will be given here as a representation. Its asymmetric unit contains only an Eu_2L_3 molecule, which consists of two Eu^{3+} ions, three L^{2-} anions, and four coordinated DMF molecules. Each Eu1 and Eu2 atom is ligated by eight oxygen atoms, among which six oxygen atoms arising from three β-diketone chelating claws and the other two oxygen atoms from two coordinated DMF molecules (Figure S12A). Like the coordination environment of Eu1 and Eu2 in Eu_2L_3, the Dy1 and Dy2 in Dy_2L_3 are also coordinated by eight oxygen atoms (Figure S12B). However, the Eu^{3+} and Dy^{3+} ions adopt different coordination geometries, that is, square antiprism (Figure 2B) and triangular dodecahedron

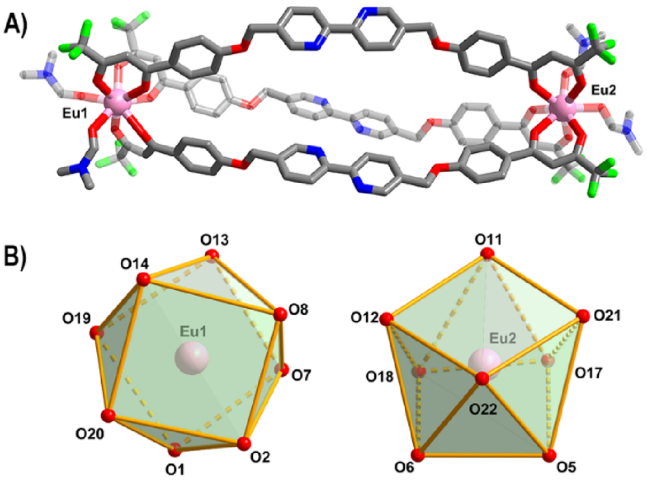

Figure 2. (A) View of the molecular structure of Eu_2L_3, hydrogen atoms were omitted for clarity. (B) Coordination geometry for Eu1 and Eu2 in Eu_2L_3 (light red: O, blue: N, pink: Eu, green: F, gray: C).

(Figure S12C) coordination geometry, respectively, as confirmed by the calculations of continuous shape measures (CShM) (Table S4).[60] Eu−O bond distances were in the range of 2.33−2.43 Å, which is comparable with other related compounds.[61] The important bond lengths and angles of Eu_2L_3 are summarized in Tables S2 and S3. Every Eu_2L_3 connects to its neighboring ones through intermolecular $\pi-\pi$ interactions in three dimensions, resulting in the formation of a supramolecular framework (Figure S13). Additionally, intermolecular hydrogen bonds are also observed in Eu_2L_3 (Figure S14). The distances of Eu···Eu within the molecule are 26.14 Å, and the nearest intermolecular Eu···Eu distances are 8.09 Å. Compared with the previously reported examples fabricated by the similar linear β-diketone ligands,[44,45] which usually possess triple-stranded helical structure characteristic, the helical feature disappeared in our cases. Given that the bpy groups are coplanar units and easy to form $\pi-\pi$ interactions among different molecules, we suggest that the absence of helix may be attributed to the introduction of the bpy unit, which weakens the spiral synergy of the three chains within one molecule.

UV−Vis, Luminescence, and Ion Recognition. The UV−vis absorption spectra of ligand H_2L and compound Eu_2L_3 are shown in Figure 3A. Compared with the free ligand H_2L, the maximum absorption wavelength of Eu_2L_3, assignable to the $\pi-\pi^*$ charge transfer transition from the aromatic group to the β-diketone units, is blue-shifted by about 27 nm (λ = 352 nm for H_2L and 325 nm for Eu_2L_3). This blue shift can be ascribed to the reduction of β-diketone chelating claw conjugation after complexation with Eu^{3+} ions, which can be confirmed by the crystal structure of Eu_2L_3. Upon excitation at 325 nm, Eu_2L_3 displays characteristic narrow line-like emission bands at 577, 591, 612, 652, and 702 nm, corresponding to $^5D_0 \rightarrow {}^7F_J$ ($J = 0-4$) transitions of Eu^{3+} (Figure 4A), among which the $^5D_0 \rightarrow {}^7F_2$ transition is a typical electric dipole transition and is very sensitive to the coordination environment of the Eu^{3+} ion. Due to the strong interaction between deporotonated β-diketonate and Eu^{3+} ion and the low symmetry of the local coordination environment without an inversion center,[62] the intensity of the electric dipole transition was enhanced, and strong red luminescence (visible to the naked eyes under the irradiation of a 365 nm UV lamp) is observed (Figure S15).

Given the metal chelator feature of the bpy moiety, the luminescence sensing properties of Eu_2L_3 toward transition metal ions were explored. Six typical transition metal ions, including Cu^{2+}, Mn^{2+}, Pb^{2+}, Ni^{2+}, Co^{2+}, and Fe^{2+}, were investigated. After the addition of transition metal ions, luminescence quenching behavior at 612 nm was distinctly observed for the investigated transition metal ions, among which Cu^{2+} is the best luminescence quenching ion (Figure 3B). Therefore, the Cu^{2+} ion was selected for luminescence titration experiments to study the mechanism of luminescence quenching by these transition metal ions (Figure 3C). In the range of 0−0.75 μM, the decrease in luminescence intensity at 612 nm displays a linear behavior with the addition of Cu^{2+} ions, from which the limit of detection (LOD) is evaluated to be 43.46 nM (2.84 ppb, S/N > 3) (Figure S16), lower than the value observed in most MOF probes.[53] The luminescence quantum lifetimes are τ_0 = 716.43 μs and τ = 711.91 μs for 0 and 3 equiv of Cu^{2+} ions (Figure S17), respectively. The ratio of τ_0/τ is very close to 1, meaning that the quenching mechanism affiliates to static quenching because dynamic quenching gives a considerable decreased lifetime, but static quenching will not change it. For static quenching, it occurs when a ground state complex is formed through the interaction between the fluorophore and quencher. Moreover, the bpy moieties usually exhibit strong chelation preference on Cu^{2+}. Hence, we speculate that the Cu^{2+} ions were coordinated to the byp unit of Eu_2L_3 and form a new complexation species, in which Cu^{2+} ions act as the quenching sites, leading to the luminescence quenching. This luminescence quenching phenomenon may be attributed to the effect of ligand to metal charge transfer (LMCT) or metal to ligand charge transfer (MLCT) on the triplet state energy level of the ligand after the formation of 1:2 host−guest complexation, which leads to the mismatch of the ligand triplet state energy level with the excited state energy level of the Eu^{3+} ion.

The UV−vis titration experiments were also performed to confirm our speculation (Figure S18). From Figure S18, we can see that the shoulder peak (285 nm) of $\pi-\pi^*$ transitions belonging to the bpy moiety decreased clearly with gradual addition of Cu^{2+} ions, and the maximum absorption peak is slightly red-shifted from 325 to 327 nm. Moreover, a new broaden absorption peak at about 355 nm appeared, which can

https://doi.org/10.1021/acsomega.3c02419
ACS Omega 2023, 8, 24477−24484

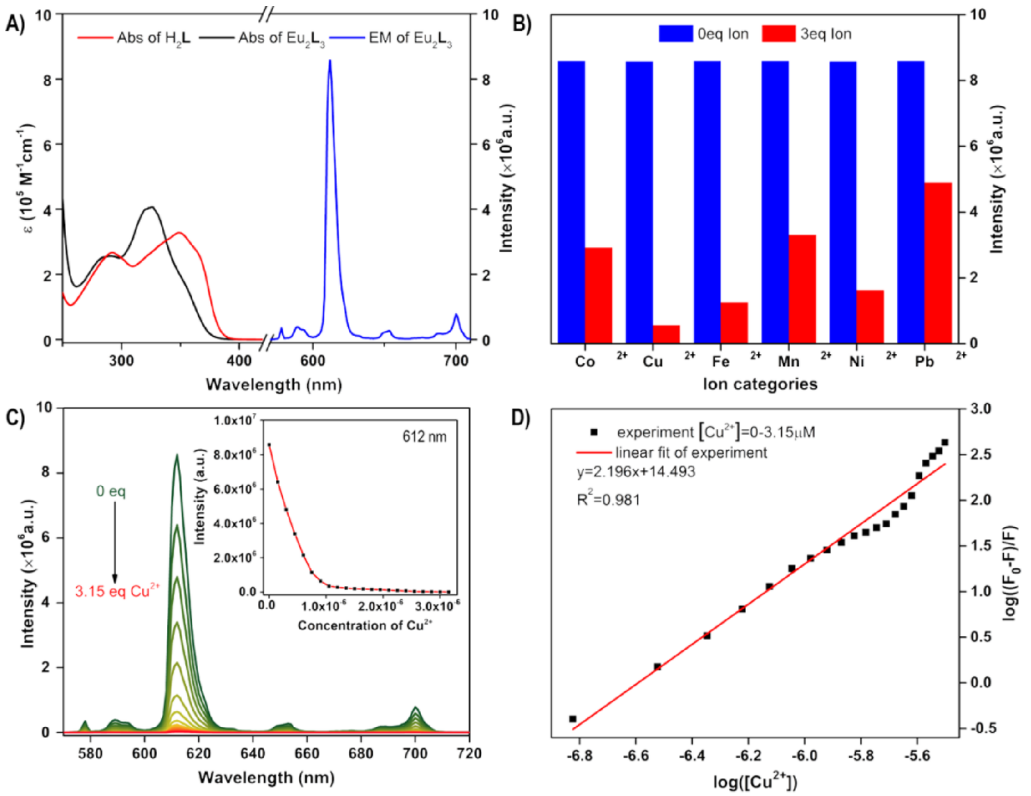

Figure 3. (A) UV−vis absorption spectra of ligands H_2**L**, compound Eu_2**L**$_3$ and the emission spectrum of compound Eu_2**L**$_3$. (B) Luminescence quenching behaviors at 612 nm after the addition of 3 equiv of different transition metal ions. (C) Luminescence titration spectra (λ_{ex} = 325 nm) of Eu_2**L**$_3$ (1.02 μM) with the addition of 0−3.21 μM of Cu^{2+} ions with the inset showing luminescence intensity change. (D) Plots of $\log((F_0 - F)/F)$ as a function of the logarithm of the Cu^{2+} concentration; the red line represents the best fit with the modified Stern−Volmer equation.

be attributed to the ligand to metal charge transfer (LMCT) or metal to ligand charge transfer (MLCT) generated by complexation of bpy with metal ions.[63] In a word, with the reduction of the absorption peak at 285 nm, the red shift of the maximum absorption band together with the appearance of the new absorption band suggests the formation of new species, in which Cu^{2+} ions are ligated to the bpy unit of Eu_2**L**$_3$, in line with our speculation. According to Cu^{2+} binding numbers, three possible products, Eu_2CuL_3, $Eu_2Cu_2L_3$, and $Eu_2Cu_3L_3$, can be anticipated, that is, the binding ratios between Eu_2**L**$_3$ and Cu^{2+} ions are 1:1, 1:2, and 1:3. To identify the possible binding ratio, the curve of $\log((F_0 - F)/F)$ vs $\log([Cu^{2+}])$ (Figure 3D) was treated by the modified Stern−Volmer equation (see the Supporting Information for details).[64−66] The best fit in the range of 0−3.15 equiv gives $K = 2.013 \times 10^{14}$ M^{-2}, $n = 2.196$ (the n value is near 2 and far less than 3), revealing that the binding ratio between the host (Eu_2**L**$_3$) and guest (Cu^{2+}) is 1:2. In addition, the result of Job's plot pointed out that the change of luminescence intensity reached the maximum when the molar fraction of (Cu^{2+}) was 0.64 (Figure S19), also corroborating the fact that the binding stoichiometry of Eu_2**L**$_3$ and Cu^{2+} is 1:2. The formation of the 1:2 host−guest compound was also testified by electrospray ionization time-of-flight mass spectroscopy (ESI-TOF-MS). After the addition of 3.0 equiv of Cu^{2+} ions, the presence of $Eu_2Cu_2L_3$ can be obviously observed in ESI-TOF-MS, and the assignments for host−guest peaks are further demonstrated by carefully comparing the simulated ones with experimental data (Figure S20). Therefore, complex $Eu_2Cu_2L_3$ with 1:2 stoichiometry between the host and guest is probably the new complexation species. The possible binding way of Cu^{2+} ions in $Eu_2Cu_2L_3$ was proposed and is shown in Figure S21. The formation of 1:2 complexation rather than 1:1 or 1:3 complexation may be caused by the steric hindrance, strong coordination ability of the bpy moiety, and relatively flexible characteristic of ligand H_2**L**.

Magnetic Property of Dy_2L_3. Direct current (dc) magnetic susceptibility measurements were performed on polycrystalline samples of the complex Dy_2**L**$_3$ in the temperature range of 300−2 K under an applied field of 1000 Oe (Figure 4A). The x_mT products are 28.90 $cm^3 \cdot K \cdot mol^{-1}$ for Dy_2**L**$_3$ at 300 K, which is close to a value of 28.34 $cm^3 \cdot K \cdot mol^{-1}$ expected for two isolated Dy^{3+} ions (J = 15/2 and g = 4/3). Upon cooling, the x_mT values exhibit a gradual decrease until 30 K, and then a sharp decrease appears, reaching the minimal values of 22.48 $cm^3 \cdot K \cdot mol^{-1}$ at 2 K. The decrease in x_mT may be caused by the thermal depopulation of the stark sublevels.[67] The $M-H$ curves of Dy_2**L**$_3$ were collected at 2, 3, and 5.0 K in the range of 0−8 T (Figure S22). As shown in the inset of Figure 3A, the M vs H/T plots are not superimposable and increase rapidly at low field and then slowly at high field regions but do not reach saturation even at 8 T, indicating the presence of magnetic anisotropy.

To certificate the presence or absence of relaxation of the magnetization, the dynamics of the magnetization for Dy_2**L**$_3$ was investigated by using alternating current susceptibility measurement under 3.0 Oe. Both the in-phase (Figure S23) and out-of-phase susceptibilities show temperature dependence behavior under a zero dc field (Figure 4B), but no peaks are observed under the measured temperature range, which

https://doi.org/10.1021/acsomega.3c02419
ACS Omega 2023, 8, 24477−24484

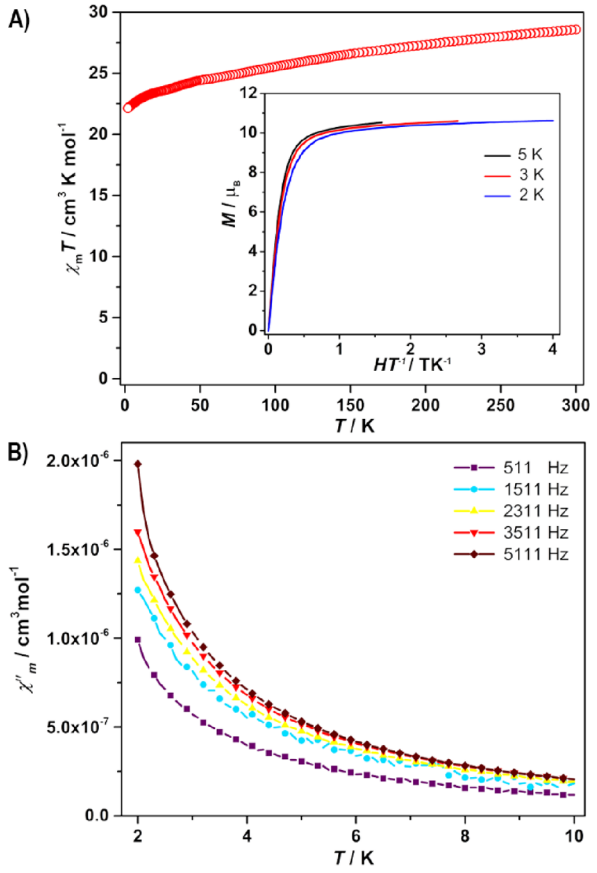

Figure 4. (A) Plots of x_mT vs T for Dy_2L_3 with the inset displaying M vs H/T at different temperatures for Dy_2L_3. (B) Temperature dependence of the out-of-phase susceptibilities for Dy_2L_3.

may suggest the presence of slow magnetic relaxation behavior. However, the contribution of fast quantum tunneling of magnetization (QTM) relaxation cannot be excluded as it can also induce the rapid increase in ac magnetic susceptibilities at low temperature range, as was commonly observed in other lanthanide magnetic relaxation systems.[68,69] To determine the energy barrier (U_{eff}) and relaxation time (τ_0), the Debye model based on the following equation was adopted[68,70]

$$\ln\left(\frac{\chi''}{\chi'}\right) = \ln(\omega\tau_0) + \frac{E_a}{k_B T} \quad (1)$$

The best-fitting affords an energy barrier (U_{eff}/K_B) of 10.03 K and τ_0 of 1.56×10^{-5} s for Dy_2L_3 under a zero dc field (Figure S24). This energy barrier is comparable to previously reported triple-stranded compounds[71,72] and is surpassed by two known Dy_2L_3-type compounds constructed by the same β-diketone chelating claw, that is, $Dy_2(MBDA)_3$ (H_2MBDA = *N*-methyl-4,4′-bis(4,4,4-trifluoro-1,3-dioxobutyl)-diphenylamine),[73] $Dy_2(BTB)_3$ (H_2BTB = 3,3′-bis(4,4,4-trifluoro-1,3-dioxobutyl)biphenyl),[44] and $Dy_2(pbth)_3$ (pbth = (3z,3′z)-4,4′-(1,3-phenylene)bis(1,1,1-trifluoro-4-hydroxybut-3-en-2-one)),[60] with energy barriers of 28.4, 20.6, and 110.2 K, respectively. Given that both Dy^{3+} ions in Dy_2L_3 are in triangular dodecahedron coordination geometry with D_{2d} symmetry, this may not favor QTM suppression.[31] Thus, the observed smaller energy barrier in Dy_2L_3 than those in $Dy_2(MBDA)_3$, $Dy_2(BTB)_3$, and $Dy_2(pbth)_3$ may be mainly attributed to the low symmetric coordination geometry of local Dy^{3+} sites.

CONCLUSIONS

In summary, Ln_2L_3-type (Ln = Eu^{3+} and Dy^{3+}) compounds were fabricated by the deprotonation self-assembly of the C_2-symmetric linear ligand containing the 2,2′-bipyridine moiety with lanthanide ions. The luminescent Eu_2L_3 compound exhibits excellent sensing performance for Cu^{2+} ions with detection limits of 43.46 nM. The luminescence sensing behavior of Eu_2L_3 was attributed to the generation of 1:2 host−guest complexation between Eu_2L_3 and Cu^{2+} ions, where Cu^{2+} ions act as the quenching sites, leading to the luminescence quenching. The magnetic measurements show that Dy_2L_3 exhibits magnetic relaxation. The results presented in this contribution offer a potential way for fabrication of lanthanide-based molecular materials with chemosensor function toward transition metal ions.

ASSOCIATED CONTENT

Supporting Information

The Supporting Information is available free of charge at https://pubs.acs.org/doi/10.1021/acsomega.3c02419.

Details of spectroscopic data (^{1}H-NMR, ^{13}C-NMR, PXRD, TG, magnetic data, UV−vis, and mass spectroscopy), experimental sections, optical properties, and crystallographic and structural data (PDF)

Crystallographic data of 2251041 and 2251298 (CIF)

Accession Codes

CCDC 2251041 and 2251298 contain the supplementary crystallographic data for this paper. These data can be obtained free of charge via www.ccdc.cam.ac.uk/data_Dy2L3 and data_Eu2L3/cif or by emailing data_request@ccdc.cam.ac.uk or by contacting the Cambridge Crystallographic Data Centre, 12 Union Road, Cambridge CB2 1EZ, UK; fax: +441223 336033.

AUTHOR INFORMATION

Corresponding Authors

Chong-Bin Tian − *College of Chemistry, Fuzhou University, Fuzhou 350108, People's Republic of China; Fujian College, University of Chinese Academy of Sciences, Fuzhou 350002, People's Republic of China;* orcid.org/0000-0002-3771-1530; Email: tianchongbin@fjirsm.ac.cn

Qing-Fu Sun − *College of Chemistry, Fuzhou University, Fuzhou 350108, People's Republic of China; Fujian College, University of Chinese Academy of Sciences, Fuzhou 350002, People's Republic of China;* orcid.org/0000-0002-6419-8904; Email: qfsun@fjirsm.ac.cn

Authors

Fan Yin − *College of Chemistry, Fuzhou University, Fuzhou 350108, People's Republic of China; Fujian College, University of Chinese Academy of Sciences, Fuzhou 350002, People's Republic of China*

Zhi Liu − *College of Chemistry, Fuzhou University, Fuzhou 350108, People's Republic of China; Fujian College, University of Chinese Academy of Sciences, Fuzhou 350002, People's Republic of China*

Jian Yang − *Fujian College, University of Chinese Academy of Sciences, Fuzhou 350002, People's Republic of China*

https://doi.org/10.1021/acsomega.3c02419
ACS Omega 2023, 8, 24477−24484

Li-Peng Zhou − *Fujian College, University of Chinese Academy of Sciences, Fuzhou 350002, People's Republic of China;* orcid.org/0000-0003-3820-2591

Complete contact information is available at: https://pubs.acs.org/10.1021/acsomega.3c02419

Author Contributions

The manuscript was written through contributions of all authors. All authors have given approval to the final version of the manuscript.

Notes

The authors declare no competing financial interest.

■ ACKNOWLEDGMENTS

This work was funded by NNSF of China (grants 21971237, 21825107, and 22171264), National Key Research and Development Program of China (grant 2021YFA1500400), and Science Foundation of Fujian Province (grants 2021J02016 and 2022J01507).

■ REFERENCES

(1) Lee, S.; Jeong, H.; Nam, D.; Lah, M. S.; Choe, W. The rise of metal-organic polyhedra. *Chem. Soc. Rev.* **2021**, *50*, 528−555.
(2) Saha, R.; Mondal, B.; Mukherjee, P. S. Molecular Cavity for Catalysis and Formation of Metal Nanoparticles for Use in Catalysis. *Chem. Rev.* **2022**, *122*, 12244−12307.
(3) Wang, H.; Li, Y.; Li, N.; Filosa, A.; Li, X. Increasing the size and complexity of discrete 2D metallosupramolecules. *Nat. Rev. Mater.* **2021**, *6*, 145−167.
(4) Wang, Z.; Zhou, L.-P.; Cai, L.-X.; Tian, C.-B.; Sun, Q.-F. From a mononuclear FeL_2 complex to a Fe_4L_4 molecular square: Designed assembly and spin-crossover property. *Nano Res.* **2021**, *14*, 398−403.
(5) Wang, W.; Wang, Y. X.; Yang, H. B. Supramolecular transformations within discrete coordination-driven supramolecular architectures. *Chem. Soc. Rev.* **2016**, *45*, 2656−2693.
(6) Gao, W. X.; Feng, H. J.; Guo, B. B.; Lu, Y.; Jin, G. X. Coordination-Directed Construction of Molecular Links. *Chem. Rev.* **2020**, *120*, 6288−6325.
(7) Gupta, G.; Sun, Y.; Das, A.; Stang, P. J.; Lee, C. Y. BODIPY based Metal-Organic Macrocycles and Frameworks: Recent Therapeutic Developments. *Coord. Chem. Rev.* **2022**, *452*, 29.
(8) McTernan, C. T.; Davies, J. A.; Nitschke, J. R. Beyond Platonic: How to Build Metal-Organic Polyhedra Capable of Binding Low-Symmetry, Information-Rich Molecular Cargoes. *Chem. Rev.* **2022**, *122*, 10393−10437.
(9) Li, X.-L.; Zhao, L.; Wu, J.; Shi, W.; Struch, N.; Lützen, A.; Powell, A. K.; Cheng, P.; Tang, J. Subcomponent self-assembly of circular helical $Dy_6(L)_6$ and bipyramid $Dy_{12}(L)_8$ architectures directed via second-order template effects. *Chem. Sci.* **2022**, *13*, 10048−10056.
(10) Habib, F.; Long, J.; Lin, P. H.; Korobkov, I.; Ungur, L.; Wernsdorfer, W.; Chibotaru, L. F.; Murugesu, M. Supramolecular architectures for controlling slow magnetic relaxation in field-induced single-molecule magnets. *Chem. Sci.* **2012**, *3*, 2158−2164.
(11) Howard-Smith, K. J.; Craze, A. R.; Zenno, H.; Yagyu, J.; Hayami, S.; Li, F. A large dinuclear Fe(II) triple helicate demonstrating a two-step spin crossover. *Chem. Commun.* **2020**, *56*, 8838−8841.
(12) Darawsheh, M.; Barrios, L. A.; Roubeau, O.; Teat, S. J.; Aromí, G. Encapsulation of a Cr^{3+} Single-Ion Magnet within an Fe^{II} Spin-Crossover Supramolecular Host. *Angew. Chem., Int. Ed.* **2018**, *57*, 13509−13513.
(13) Cai, L. X.; Yan, L. L.; Li, S. C.; Zhou, L. P.; Sun, Q. F. Stereocontrolled self-assembly and photochromic transformation of lanthanide supramolecular helicates. *Dalton Trans.* **2018**, *47*, 14204−14210.
(14) Zhou, Y.; Yao, Y.; Cheng, Z.; Gao, T.; Li, H.; Yan, P. Point Chirality Controlled Diastereoselective Self-Assembly and Circularly Polarized Luminescence in Quadruple-Stranded Europium(III) Helicates. *Inorg. Chem.* **2020**, *59*, 12850−12857.
(15) Bassett, A. P.; Magennis, S. W.; Glover, P. B.; Lewis, D. J.; Spencer, N.; Parsons, S.; Williams, R. M.; De Cola, L.; Pikramenou, Z. Highly luminescent, triple- and quadruple-stranded, dinuclear Eu, Nd, and Sm(III) lanthanide complexes based on bis-diketonate ligands. *J. Am. Chem. Soc.* **2004**, *126*, 9413−9424.
(16) Zare, D.; Suffren, Y.; Nozary, H.; Hauser, A.; Piguet, C. Controlling Lanthanide Exchange in Triple-Stranded Helicates: A Way to Optimize Molecular Light-Up conversion. *Angew. Chem., Int. Ed.* **2017**, *56*, 14612−14617.
(17) Hrabina, O.; Malina, J.; Kostrhunova, H.; Novohradsky, V.; Pracharova, J.; Rogers, N.; Simpson, D. H.; Scott, P.; Brabec, V. Optically Pure Metallohelices That Accumulate in Cell Nuclei, Condense/Aggregate DNA, and Inhibit Activities of DNA Processing Enzymes. *Inorg. Chem.* **2020**, *59*, 3304−3311.
(18) Li, Y.; Yang, T.; Li, N.; Bai, S.; Li, X.; Ma, L.-L.; Wang, K.; Zhang, Y.; Han, Y.-F. Multistimuli-Responsive Fluorescent Organometallic Assemblies Based on Mesoionic Carbene-Decorated Tetraphenylethene Ligands and Their Applications in Cell Imaging. *CCS Chem.* **2022**, *4*, 732−743.
(19) Chen, R.; Yan, Q.-Q.; Hu, S.-J.; Guo, X.-Q.; Cai, L.-X.; Yan, D.-N.; Zhou, L.-P.; Sun, Q.-F. Dinuclear helicate or mononuclear pincer lanthanide complexes from one ligand: stereo-controlled assembly and catalysis. *Org. Chem. Front.* **2021**, *8*, 2576−2582.
(20) Chu, D.; Gong, W.; Jiang, H.; Tang, X.; Cui, Y.; Liu, Y. Boosting Enantioselectivity of Chiral Molecular Catalysts with Supramolecular Metal-Organic Cages. *CCS Chem.* **2022**, *4*, 1180−1189.
(21) Guo, X. Q.; Zhou, L. P.; Hu, S. J.; Cai, L. X.; Cheng, P. M.; Sun, Q. F. Hexameric Lanthanide-Organic Capsules with Tertiary Structure and Emergent Functions. *J. Am. Chem. Soc.* **2021**, *143*, 6202−6210.
(22) Cui, F.; Li, S.; Jia, C.; Mathieson, J. S.; Cronin, L.; Yang, X.-J.; Wu, B. Anion-Dependent Formation of Helicates versus Mesocates of Triple-Stranded M_2L_3 (M = Fe^{2+}, Cu^{2+}) Complexes. *Inorg. Chem.* **2012**, *51*, 179−187.
(23) Jiao, J.; Dong, J.; Li, Y.; Cui, Y. Fine-Tuning of Chiral Microenvironments within Triple-Stranded Helicates for Enhanced Enantioselectivity. *Angew. Chem., Int. Ed.* **2021**, *60*, 16568−16575.
(24) Lehn, J. M.; Rigault, A.; Siegel, J.; Harrowfield, J.; Chevrier, B.; Moras, D. Spontaneoua assembly of bouble-stranded helicates from oligobipyriaine ligands and copper(1) cations- structure of an inorganic double helix. *Proc. Natl. Acad. Sci. U. S. A.* **1987**, *84*, 2565−2569.
(25) Piguet, C.; Borkovec, M.; Hamacek, J.; Zeckert, K. Strict self-assembly of polymetallic helicates: the concepts behind the semantics. *Coord. Chem. Rev.* **2005**, *249*, 705−726.
(26) Tran, N. M.; Yoo, H. Recent advances in heteroleptic multiple-stranded metallosupramolecules. *Dalton Trans.* **2020**, *49*, 11819−11827.
(27) Albrecht, M. "Let's twist again" - Double-stranded, triple-stranded, and circular helicates. *Chem. Rev.* **2001**, *101*, 3457−3498.
(28) Piguet, C.; Bernardinelli, G.; Hopfgartner, G. Helicates as versatile supramolecular complexes. *Chem. Rev.* **1997**, *97*, 2005−2062.
(29) Li, X. Z.; Tian, C. B.; Sun, Q. F. Coordination-Directed Self-Assembly of Functional Polynuclear Lanthanide Supramolecular Architectures. *Chem. Rev.* **2022**, *122*, 6374−6458.
(30) Bünzli, J. C. G.; Piguet, C. Taking advantage of luminescent lanthanide ions. *Chem. Soc. Rev.* **2005**, *34*, 1048−1077.
(31) Liu, J. L.; Chen, Y. C.; Tong, M. L. Symmetry strategies for high performance lanthanide-based single-molecule magnets. *Chem. Soc. Rev.* **2018**, *47*, 2431−2453.
(32) Zhu, Z.; Tang, J. Metal-metal bond in lanthanide single-molecule magnets. *Chem. Soc. Rev.* **2022**, *51*, 9469−9481.
(33) Lu, J.; Li, X.-L.; Zhu, Z.; Liu, S.; Yang, Q.; Tang, J. Linear hexanuclear helical dysprosium single-molecule magnets: the effect of

axial substitution on magnetic interactions and relaxation dynamics. *Dalton Trans.* **2019**, *48*, 14062−14068.
(34) Zhang, Y.; Ali, B.; Wu, J.; Guo, M.; Yu, Y.; Liu, Z.; Tang, J. Construction of Metallosupramolecular Coordination Complexes: From Lanthanide Helicates to Octahedral Cages Showing Single-Molecule Magnet Behavior. *Inorg. Chem.* **2019**, *58*, 3167−3174.
(35) Hamacek, J.; Blanc, S.; Elhabiri, M.; Leize, E.; Van Dorsselaer, A.; Piguet, C.; Albrecht-Gary, A. M. Self-assembly mechanism of a bimetallic europium triple-stranded helicate. *J. Am. Chem. Soc.* **2003**, *125*, 1541−1550.
(36) Zeckert, K.; Hamacek, J.; Senegas, J. M.; Dalla-Favera, N.; Floquet, S.; Bernardinelli, G.; Piguet, C. Predictions, synthetic strategy, and isolation of a linear tetrametallic triple-stranded lanthanide helicate. *Angew. Chem., Int. Ed.* **2005**, *44*, 7954−7958.
(37) Chauvin, A.-S.; Comby, S.; Song, B.; Vandevyver, C. D. B.; Thomas, F.; Bünzli, J.-C. G. A polyoxyethylene-substituted bimetallic europium helicate for luminescent staining of living cells. *Chem. − Eur. J.* **2007**, *13*, 9515−9526.
(38) Bünzli, J. C. G.; Piguet, C. Lanthanide-containing molecular and supramolecular polymetallic functional assemblies. *Chem. Rev.* **2002**, *102*, 1897−1928.
(39) El Aroussi, B.; Zebret, S.; Besnard, C.; Perrottet, P.; Hamacek, J. Rational Design of a Ternary Supramolecular System: Self-Assembly of Pentanuclear Lanthanide Helicates. *J. Am. Chem. Soc.* **2011**, *133*, 10764−10767.
(40) Johnson, A. M.; Wiley, C. A.; Young, M. C.; Zhang, X.; Lyon, Y.; Julian, R. R.; Hooley, R. J. Narcissistic Self-Sorting in Self-Assembled Cages of Rare Earth Metals and Rigid Ligands. *Angew. Chem., Int. Ed.* **2015**, *54*, 5641−5645.
(41) Johnson, A. M.; Young, M. C.; Zhang, X.; Julian, R. R.; Hooley, R. J. Cooperative Thermodynamic Control of Selectivity in the Self-Assembly of Rare Earth Metal-Ligand Helices. *J. Am. Chem. Soc.* **2013**, *135*, 17723−17726.
(42) Zhao, L.; Liu, Y.; He, C.; Wang, J.; Duan, C. Coordination-driven nanosized lanthanide 'Molecular Lanterns' as luminescent chemosensors for the selective sensing of magnesium ions. *Dalton Trans.* **2014**, *43*, 335−343.
(43) Zhu, X.; He, C.; Dong, D.; Liu, Y.; Duan, C. Cerium-based triple-stranded helicates as luminescent chemosensors for the selective sensing of magnesium ions. *Dalton Trans.* **2010**, *39*, 10051−10055.
(44) Li, H.; Chen, P.; Sun, W.; Zhang, L.; Yan, P. Solvent triggered structural diversity of triple-stranded helicates: single molecular magnets. *Dalton Trans.* **2016**, *45*, 3175−3181.
(45) Zhang, J.; Zhou, Y.; Yao, Y.; Cheng, Z.; Gao, T.; Li, H.; Yan, P. A light triggered optical and chiroptical switch based on a homochiral Eu_2L_3 helicate. *J. Mater. Chem. C* **2020**, *8*, 6788−6796.
(46) Liu, C. L.; Zhou, L. P.; Tripathy, D.; Sun, Q. F. Self-Assembly of Stable Luminescent Lanthanide Supramolecular M_4L_6 Cage with Sensing Properties toward Nitroaromatics. *Chem. Commun.* **2017**, *53*, 2459−2462.
(47) Li, X.-Z.; Zhou, L.-P.; Yang, L.-L.; Yuan, D.-Q.; Lin, C.-S.; Sun, Q.-F. Evolution of Luminescent Supramolecular Lanthanide M2nL3n Complexes from Helicates and Tetrahedra to Cubes. *J. Am. Chem. Soc.* **2017**, *139*, 8237−8244.
(48) Shu, Y. B.; Tang, X. L.; Liu, W. S. Sm and Eu(III) lanthanide triple helicate cages based on N,N '-methylene-bis(pyridin-4-one). *Inorg. Chem. Front.* **2014**, *1*, 226−230.
(49) Yim, K.-H.; Yeung, C.-T.; Probert, M. R.; Chan, W. T. K.; Mackenzie, L. E.; Pal, R.; Wong, W.-T.; Law, G.-L. Helicate-to-tetrahedron transformation of chiral lanthanide supramolecular complexes induced by ionic radii effect and linker length. *Commun. Chem.* **2021**, *4*, 10.
(50) Barry, D. E.; Kitchen, J. A.; Pandurangan, K.; Savyasachi, A. J.; Peacock, R. D.; Gunnlaugsson, T. Formation of Enantiomerically Pure Luminescent Triple-Stranded Dimetallic Europium Helicates and Their Corresponding Hierarchical Self-Assembly Formation in Protic Polar Solutions. *Inorg. Chem.* **2020**, *59*, 2646−2650.
(51) Brock, A. J.; Etchells, I. M.; Moore, E. G.; Clegg, J. K. Dinuclear triple stranded phenyl-spaced 1,3-bis-beta-diketonato lanthanide(III) complexes: synthesis, structures and spectroscopy. *Dalton Trans.* **2021**, *50*, 4874−4879.
(52) Hancock, R. D. The pyridyl group in ligand design for selective metal ion complexation and sensing. *Chem. Soc. Rev.* **2013**, *42*, 1500−1524.
(53) Lin, X.; Hong, Y.; Zhang, C.; Huang, R.; Wang, C.; Lin, W. Pre-concentration and energy transfer enable the efficient luminescence sensing of transition metal ions by metal-organic frameworks. *Chem. Commun.* **2015**, *51*, 16996−16999.
(54) Tu, T. N.; Nguyen, M. V.; Nguyen, H. L.; Yuliarto, B.; Cordova, K. E.; Demir, S. Designing bipyridine-functionalized zirconium metal-organic frameworks as a platform for clean energy and other emerging applications. *Coord. Chem. Rev.* **2018**, *364*, 33−50.
(55) Qian, Z.; Cheng, Y.; Zhao, S.; Wong, K. M. C. Design, Synthesis and Ring-Opening Properties of a New Bipyridine Fused Rhodamine-Like Chelating Ligand and the Related Transition Metal Complexes(dagger). *Chin. J. Chem.* **2021**, *39*, 1659−1666.
(56) Hoffrichter, G.; Lützen, A. Allosteric binding of sodium deoxycholate by a bis(beta-cyclodextrin)-2,2′-bipyridine receptor. *Org. Chem. Front.* **2021**, *8*, 5810−5820.
(57) Jiang, S. D.; Wang, B. W.; Su, G.; Wang, Z. M.; Gao, S. A Mononuclear Dysprosium Complex Featuring Single-Molecule-Magnet Behavior. *Angew. Chem., Int. Ed.* **2010**, *49*, 7448−7451.
(58) Divya, K. P.; Sreejith, S.; Balakrishna, B.; Jayamurthy, P.; Anees, P.; Ajayaghosh, A. A Zn^{2+}-specific fluorescent molecular probe for the selective detection of endogenous cyanide in biorelevant samples. *Chem. Commun.* **2010**, *46*, 6069−6071.
(59) Peters, J. A.; Huskens, J.; Raber, D. J. Lanthanide induced shifts and relaxation rate enhancements. *Prog. Nucl. Magn. Reson. Spectrosc.* **1996**, *28*, 283−350.
(60) Tang, J.; Zhang, S.; Li, L.; Yao, L.; Zhang, R.; Yin, B.; Zhang, J. Influence of ligand substitution and the solvent effect on the structures and magnetic properties of dinuclear Dy_2 supramolecular architectures constructed with the bis-beta-diketonate-Dy-2 building block as a metalloligand. *Dalton Trans.* **2023**, *52*, 1366−1377.
(61) Du, M.-H.; Chen, L.-Q.; Jiang, L.-P.; Liu, W.-D.; Long, L.-S.; Zheng, L.; Kong, X.-J. Counterintuitive Lanthanide Hydrolysis-Induced Assembly Mechanism. *J. Am. Chem. Soc.* **2022**, *144*, 5653−5660.
(62) Kitagawa, Y.; Ueda, J.; Fujii, K.; Yashima, M.; Funahashi, S.; Nakanishi, T.; Takeda, T.; Hirosaki, N.; Hongo, K.; Maezono, R.; Tanabe, S. Site-Selective Eu^{3+} Luminescence in the Monoclinic Phase of $YSiO_2N$. *Chem. Mater.* **2021**, *33*, 8873−8885.
(63) Baskin, M.; Maayan, G. Chiral Cu(II), Co(II) and Ni(II) complexes based on 2,2′-bipyridine modified peptoids. *Dalton Trans.* **2018**, *47*, 10767−10774.
(64) Liu, W. H.; Wang, Y.; Tang, J. H.; Shen, G. L.; Yu, R. Q. An optical fiber sensor for berberine based on immobilized 1,4-bis(naphth 2,1-d oxazole-2-yl)benzene in a new copolymer. *Talanta* **1998**, *46*, 679−688.
(65) Xia, X. L.; Zhang, D. B.; Zhang, J. L.; Pu, S. Z. Highly sensitive ruthenium complex-based fluorescent probe for copper ion detection. *Tetrahedron* **2020**, *76*, No. 131526.
(66) Li, C. Y.; Zhang, X. B.; Jin, Z.; Han, R.; Shen, G. L.; Yu, R. Q. A fluorescent chemosensor for cobalt ions based on a multi-substituted phenol-ruthenium(II) tris(bipyridine) complex. *Anal. Chim. Acta* **2006**, *580*, 143−148.
(67) Wu, J.; Zhao, L.; Zhang, L.; Li, X. L.; Guo, M.; Powell, A. K.; Tang, J. Macroscopic Hexagonal Tubes of 3d-4f Metallocycles. *Angew. Chem., Int. Ed.* **2016**, *55*, 15574−15578.
(68) Lu, J.; Montigaud, V.; Cador, O.; Wu, J.; Zhao, L.; Li, X. L.; Guo, M.; Le Guennic, B.; Tang, J. Lanthanide(III) Hexanuclear Circular Helicates: Slow Magnetic Relaxation, Toroidal Arrangement of Magnetic Moments, and Magnetocaloric Effects. *Inorg. Chem.* **2019**, *58*, 11903−11911.
(69) Meng, Z. S.; Guo, F. S.; Liu, J. L.; Leng, J. D.; Tong, M. L. Heterometallic cubane-like {M2Ln2} (M = Ni, Zn; Ln = Gd, Dy) and

https://doi.org/10.1021/acsomega.3c02419
ACS Omega 2023, 8, 24477−24484

{Ni2Y2} aggregates. Synthesis, structures and magnetic properties. *Dalton Trans.* **2012**, *41*, 2320−2329.
(70) Bartolomé, J.; Filoti, G.; Kuncser, V.; Schinteie, G.; Mereacre, V.; Anson, C. E.; Powell, A. K.; Prodius, D.; Turta, C. Magneto-structural correlations in the tetranuclear series of $\{Fe_3LnO_2\}$butterfly core clusters: Magnetic and Mössbauer spectroscopic study. *Phys. Rev. B* **2009**, *80*, No. 014430.
(71) Lin, S.-Y.; Xu, G.-F.; Zhao, L.; Guo, Y.-N.; Guo, Y.; Tang, J. Observation of slow magnetic relaxation in triple-stranded lanthanide helicates. *Dalton Trans.* **2011**, *40*, 8213−8217.
(72) Gao, X.; Li, H.; Chen, P.; Sun, W.; Yan, P. A series of triple-stranded lanthanide(III) helicates: syntheses, structures and single molecular. *Polyhedron* **2017**, *126*, 1−7.
(73) Chen, P.; Li, H.; Sun, W.; Tang, J.; Zhang, L.; Yan, P. Crystallization of triple- and quadruple-stranded dinuclear bis-β-diketonate-Dy(III) helicates: single molecule magnetic behavior. *CrystEngComm* **2015**, *17*, 7227−7232.

https://doi.org/10.1021/acsomega.3c02419
ACS Omega 2023, 8, 24477−24484